IEEE Access
Multidisciplinary | Rapid Review | Open Access Journal

Received November 5, 2018, accepted November 26, 2018, date of publication November 29, 2018,
date of current version December 27, 2018.

Digital Object Identifier 10.1109/ACCESS.2018.2883988

Induction Motor Failure Analysis: An Automatic Methodology Based on Infrared Imaging

EMMANUEL RESENDIZ-OCHOA, ROQUE A. OSORNIO-RIOS, (Member, IEEE), JUAN PRIMO BENITEZ-RANGEL, RENE DE J. ROMERO-TRONCOSO, (Senior Member, IEEE), AND LUIS ALBERTO MORALES-HERNANDEZ, (Member, IEEE)

Mecatrónica/Facultad de Ingeniería, Universidad Autónoma de Querétaro, Campus San Juan del Rio, Queretaro 76807, Mexico

Corresponding author: Luis A. Morales-Hernandez (lamorales@hspdigital.org)

This work was partially supported by CONACyT scholarship 296882. This paper was supported for publication with resources PFCE2018.

ABSTRACT The main techniques used for failure analysis in induction motors are limited because they are not capable of detecting all the faults present in an induction motor. However, a complementary technique that aids in fault diagnosis in induction motors is infrared imaging. This paper proposes an automatic methodology based on infrared imaging for thermal condition monitoring and failure analysis in induction motors and the kinematic chain; it can be considered an alternative tool for classical infrared imaging inspection procedures and for monitoring and failure analysis techniques in an induction motor in particular. The proposed methodology detects the region of interest using automatic image segmentation by means of the Otsu thresholding method, where it performs the feature extraction of temperatures for the thermal analysis of induction motors. The methodology is based on the standard ASTM E1934-99a for fault diagnosis in induction motors. To demonstrate the efficiency of the proposed methodology, this paper presents the failure analysis of three fault conditions in an induction motor: a broken rotor bar, bearing damage, and misalignment.

INDEX TERMS Induction motor, infrared imaging, condition monitoring, failure analysis, image segmentation, thermal analysis.

I. INTRODUCTION

Induction motors (IM) are electric machines that are used for a variety of purposes in industrial plants [1], [2]. IM represent 85% of the worldwide energy consumption due to their robustness, low cost and versatility [3]. However, IM are subject to undesirable fatigue and stress, which can cause machine damage or failure [4]. For this reason, condition monitoring and fault diagnosis in IM receive considerable attention, resulting in new techniques and methodologies for fault location in IM. The most common faults in IM are reported to be 41% due to ball bearing damage (BD), 37% due to stator faults, 10% due to rotor faults and 12% attributed to other failure types [5]. When an IM is operated with a fault, its operational costs increase. Consequently, failure analysis of IM is one of the most important topics in industry applications [1]. For condition monitoring and fault diagnosis in IM, different techniques and methodologies are used for inspection. However, these techniques used have their own limitations and are not capable of diagnosing all the faults present in the IM. The most commonly used techniques are temperature measurement, vibration, electrical signals (MCSA) and acoustic measurement [6]–[9].

A complementary technique that has been emerging as an aid in fault diagnosis in IM is infrared imaging, a non-invasive and nondestructive technique that efficiently monitors temperature. Qualitative and quantitative analysis using infrared imaging represents a large area of opportunity for the development of new failure analysis methodologies [10]. The goals of condition monitoring in IM are to reduce associated dangers, maximize the availability of the rotating machines, and provide forewarning of some unforeseen faults, since enormous economic costs of operation may arise when these types of factors are not considered [11], [12]. Infrared imaging has become important in preventive and predictive maintenance scheduling because it is possible to visualize and locate hot spots or a region of interest (ROI) to determine maloperation conditions and then establish a criterion for monitoring, fault detection and fault diagnosis in electromechanical systems [11]–[14]. An increase in temperature is a possible symptom of fault detection in IM, due to the problem

that causes the high temperature in the rotating machine components. In addition, the fault can affect other components in the kinematic chain, increasing their temperatures, a situation that can be detected with infrared imaging. Inspections can be carried out while the equipment is operating, preventing risks [14], [15] and globally monitoring the IM and their kinematic chains by locating ROIs where the temperature has increased.

Different methods for detecting ROIs have been used in multiple applications. One of these is the Otsu thresholding method, selected for use in this research due to its performance in different infrared imaging applications as reported in the literature. For example, in the field of medicine, image segmentation detects regions that represent breast cancer [16]; in materials testing, image segmentation is used to detect surface cracks in titanium-coated aluminum [17]; and in electrical equipment, image segmentation is used to inspect switches, fuses, and substations [18].

However, one of the problems with infrared imaging is that most of the proposed methodologies are performed either manually or semiautomatically with the help of commercial software and depend on an expert technician, which may result in lost time, greater human effort and higher economic cost. For this reason, the proposal of new automatic methodologies based on infrared imaging can be a helpful tool for preventive and predictive maintenance in the industrial sector, reducing analysis time, economic cost, and human effort [11].

In the literature, different methodologies are reported for monitoring IM thermal factors. The majority of methodologies that use infrared imaging for condition monitoring of IM aim to estimate damage by analyzing the thermal behavior of the electric machine. These methodologies analyze the performance curve for energy balance and calculate heat losses or perform condition monitoring of IM during transient states [19]–[22]. Other methods monitor the insulation degradation in the stator [23]. It is also possible to detect cooling system failure in IM by infrared imaging [24]. More recently, infrared imaging has been used to study the most common faults present in IM such as broken rotor bars, damaged ball bearings, misalignment, inappropriate connections, etc. [25]–[29].

Infrared imaging has been combined with image processing techniques to identify ROIs by applying thresholds for detecting stator winding interturn faults in an IM [27], ball bearing defects [28], or for other mechanical factors [29]. However, these methodologies are based on manual or semiautomatic methods requiring expert knowledge for infrared imaging analysis, as well as the support of commercial software to analyze the thermal image temperature measurement, which also depends on trained personnel, and has an associated data processing time as well as greater human and economic costs.

This paper is based on a previously proposed methodology [28], which consists of thermal condition monitoring of IM using infrared imaging. The image is segmented and feature extraction of the parameters of interest in the ROI is conducted for failure analysis. The methodology is applied only to the study of ball bearing defect faults, and has the inconvenience of requiring commercial software, data processing time and human effort to apply the methodology. However, in order to reduce the inconveniences of the previous methodology, this work proposes a methodology to detect the ROI of some faults in IM (ball bearing defects, broken rotor bars, and misalignment) using automatic segmentation of the infrared image. Within the ROI, failure analysis and diagnosis in the IM is realized based on thermal analysis. With this proposal, it is possible to eliminate dependence on the visual interpretation of the thermographic camera operator, which then becomes a support tool for failure analysis and diagnosis in IM. A thermographic camera is used for thermal condition monitoring of the IM, detecting the ROI in the infrared image by means of the Otsu thresholding method, which is proposed for image segmentation. Next, the thermogram is calculated from the gray-scale intensity values of the infrared image; with the ROI and the thermogram, feature extraction (maximum temperature, minimum temperature, average temperature, relative temperature, temperature difference and heating area) is performed and first order statistical parameters are calculated and used for failure analysis in IM. A qualitative method is applied, and based on the ASTM E1934-99a standard, fault diagnosis in IM is determined to estimate the severity of the fault. Finally, the efficiency of the methodology is proven through the analysis of three types of faults: ball bearing defects (BD), broken rotor bars (BRB), and misalignment (MAL) in IM with associated kinematic chains to analyze the behavior and mechanism of failure in IM.

II. THEORETICAL CONSIDERATIONS

A. INFRARED THERMOGRAPHY AND EMISSIVITY

An infrared thermography camera absorbs the infrared radiation emitted by a body with a noncontact method, and using Stefan-Boltzmann's law, the body temperature is obtained [30]. The camera measures an apparent temperature which must be corrected with the known surface emissivity.

The maximum radiant power that can be emitted by any object depends only on the temperature of the object with the thermal radiation.

The radiance spectra emitted by a surface with a temperature T and a wavelength λ is given by Planck's law (1).

$$M(\lambda, T) = \frac{C_1}{\lambda^5 (exp^{\left(C_2/\lambda T\right)} - 1)} \tag{1}$$

Where,

$$C_1 = 2\pi hc^2 = 3.742x10^8 W \cdot \mu m/m^2$$
$$C_2 = hc/k = 1.439x10^4\ \mu m \cdot K$$

$M(\lambda, T)$ is given in $\left(W/m^2.\mu m\right)$, T is the absolute temperature of the surface in Kelvin and λ is the wavelength. The wavelength of peak transmission in this representation

is found by locating the maximum via of the condition. This leads to Wien's displacement law (2).

$$\lambda_{max} \cdot T = 2897.8\ \mu m \cdot K \tag{2}$$

The spectral emission of a blackbody source is calculated from Stefan-Boltzmann's law (3).

$$M_{BB}(\lambda, T) = \int_0^{\infty} M_{\lambda}(T)\, d\lambda = \frac{\sigma T^4}{\lambda} \tag{3}$$

Here, $M_{BB}(\lambda, T)$ is given in $\left({}^{W}/_{m^2 \cdot \mu m}\right)$ and $\sigma = 5.67 \times 10^{-8} W/m^2 \cdot K^4$ denotes the Stefan-Boltzmann constant.

The emissivity of a surface represents the ratio between the radiation emitted by the surface at a given temperature and the radiation emitted by a blackbody at the same temperature. The emissivity of a surface (ε) varies between 0 and 1, inclusively.

To estimate the spectral hemispherical emissivity, the wavelength and average direction (4) is applied. The emissivity of a surface at a given wavelength can be different at different temperatures, since the spectral distribution of the emitted radiation changes with the temperature.

$$\varepsilon(\lambda, T) = \frac{M(\lambda, T)}{M_{BB}(\lambda, T)} \tag{4}$$

Due to the difficulty of guessing accurate values for emissivity, it is a common practice to directly measure ε. The easiest method is to attach tape or a paint with a known emissivity to the object under study. In the analysis, the surface temperatures of the tape or paint follow from their known ε. Assuming good thermal contact and waiting until thermal equilibrium is established, adjacent surface temperatures of the object are assumed to be the same; hence, the object emissivity is found by varying ε in the camera software until the object temperature is equal to the known tape surface temperature. The accuracy of this method depends on the accuracy of the known emissivity [31], [32].

B. INFRARED IMAGE SEGMENTATION WITH THE AUTOMATIC THRESHOLD METHOD

Infrared image segmentation is the division of an image into regions or categories corresponding to different objects or parts of objects [33]–[35]. It is possible to perform the segmentation manually or automatically. The threshold method is used for automatic infrared image segmentation (5), and it consists of the separation of hot regions from the rest of the image, comparing with an original infrared image, *I(x, y)*. For this method, a threshold value U between 0 and 255 is proposed for the threshold of an 8-bit gray-scale image.

$$G(x, y) = \left\{ \begin{array}{c} 255\ if\ I(x, y) > U \\ 0\ if\ I(x, y) \leq U \end{array} \right\} \tag{5}$$

where U is the proposed threshold value. The value of 255 represents the zone of the region of interest (ROI) or heat, 0 represents the bottom of the image and *G (x, y)* represents the result of the threshold.

The Otsu threshold method is applied to obtain an automatic segmentation (6); the objective of these methods is to find the ideal threshold value that best adapts to the infrared image under consideration [36].

$$U_{opt} = \arg\max \left\{ \frac{P_o\,[1 - P_o]\,[\mu_f - \mu_o]^2}{\left[P_o \sigma_f^2\right] + [1 - P_o]\sigma_o^2} \right\} \tag{6}$$

where U_{opt} is the optimal threshold parameter for obtaining automatic segmentation, μ_o and μ_f represent the mean value of the hot region and the background respectively, σ_o is the standard deviation for the background image, σ_f is the standard deviation for the hot region, P_o is cumulative probability $P_o = \sum_{i=0}^{U} p(i)$, where $p(i) = \frac{n_i}{N}$, $p(i)$ is the histogram probability distribution of the image, n_i is the gray level frequency i, N is the total number of pixels and U is a proposed threshold.

C. MOTOR FAULTS AND THERMAL RELATIONSHIP

Some of the most studied fault conditions in IM are ball bearing defects and broken rotor bars. BD result from poor bearing lubrication or abnormal friction in the bearing housing. This causes an increase in temperature in the area where the bearing is installed [37], which propagates into the induction motor and other parts of the kinematic chain. BRB occur when the bars inside the rotor armor experience partial or total breakage. This fault appears because of welding defects, high strength joints, hot spots, and mechanical stress [25]. When joint resistance occurs in a bar, heat dissipation takes place around that point. This fault propagates to adjacent bars due to the increment of current and temperature, accelerating the damage in the electric machine [25] and consequently that of other elements in the kinematic chain. MAL is present when the rotating machine shaft and the load pulleys are not aligned; this fault can be expressed as an eccentricity in the induction motor, which generates more mechanical stress and excessive rubbing and fatigue of the ball bearings, causing decrease in torque, reduction in efficiency and increase in temperature in the electric machine [38].

III. METHODOLOGY

This section describes the automatic methodology proposed for the monitoring, detection and feature extraction of the shape of the ROI and the parameters of interest during infrared imaging application to thermal analysis in IM. The methodology is described in five steps as shown in Fig. 1. In the first step, the electromechanical system to be monitored is identified, which, for this work, consists of an induction motor with an associated kinematic chain. The second step of thermal condition monitoring with infrared imaging is identifying the system of interest; the calibration and validation of measurements are performed with an RTD (Resistance Temperature Detector).

The third is the detection of the ROI automatically through image segmentation using the Otsu threshold method. In the

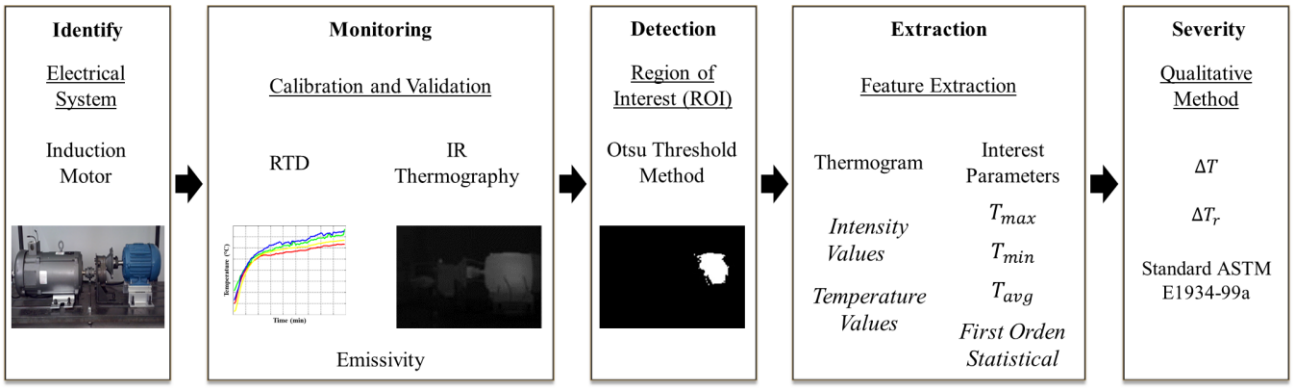

FIGURE 1. Proposed automatic methodology for induction motor failure analysis based on infrared imaging.

fourth step, the feature extraction is obtained, the thermogram (temperature matrix) is calculated from the intensity values of the infrared imaging and the parameters of interest are extracted. Last, the severity of the fault is estimated using failure analysis based on a qualitative method and the ASTM E1934-99a standard.

A. IDENTIFY THE ELECTROMECHANICAL SYSTEM FOR MONITORING

The first step is to identify the electromechanical system which will be monitored; for this work, an induction motor and its associated kinematic chain are used to determine the hot spots produced by the equipment operating conditions. Once the system to be monitored has been identified, it is possible to establish the operation to propose different cases of study for the electric machine.

B. MONITORING

In this step, an infrared thermography camera is used for thermal condition monitoring of the rotating machine and its neighboring kinematic chain. This camera can be used in several temperature ranges depending on the emissivity of the surface. With the image capture, two additional images can be obtained: first, a pseudocolored thermal image that allows the human eye to observe the heat distribution in the IM being monitored, and second, a gray-scale infrared image which is used by the proposed methodology.

A calibration and validation of the thermographic camera's temperature values is performed. For the calibration, the temperature values obtained with the thermographic camera are compared with the output of a comparative method. Several RTD temperature sensors were used to obtain the reference measurement. The calibration guarantees that the measurement obtained with the thermographic camera is the same as that of the equipment to be monitored.

First, the RTD temperature sensors are installed inside the IM in different places (T2-T7) as depicted in Fig. 2, while another RTD sensor is used to measure the ambient temperature (T1). Then, the measurements of the thermography

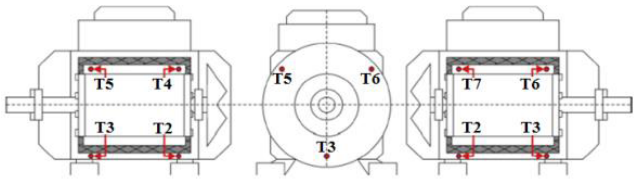

FIGURE 2. Location of temperature sensors (RTD) inside the induction motor as a temperature reference measurement for calibration and validation of the thermography camera.

camera are adjusted based on the mean temperature of the RTD.

In addition, the emissivity is theoretically calculated from the temperature (T) measured by the RTD in Kelvin and the wavelength (λ) obtained by Wien's displacement law. With the values of T and λ, the radiance spectra emitted by a surface is calculated by Planck's law; the spectral emission of a blackbody is determined with the Stefan-Boltzmann law. Finally, with the values obtained, the emissivity (ε) is estimated using the equation of spectral hemispherical emissivity (4).

This value is then adjusted by empirical tests and supervised adjustment, by placing a piece of adhesive tape of known emissivity on the induction motor, and then monitoring the IM with the thermographic camera, recording infrared imaging adjusted to the coefficient of emissivity of the adhesive tape. The thermography reads the temperature of the tape, then another area of the IM without adhesive tape is measured and the coefficient of emissivity of the thermographic camera is changed until the temperature of that area of the IM is the same as that previously registered with the adhesive tape [31].

C. DETECTION

Thresholding is a widely used method in image segmentation for detecting the ROI in infrared imaging either manually or automatically. Manual thresholding requires much time and more human effort than automatic thresholding. Therefore, the Otsu threshold is proposed as an automatic tool to detect the ROI in induction motors under different fault conditions.

The proposed methodology works with gray-scale infrared imaging. The histogram that identifies the intensity distribution of the pixels that agree with gray-scale infrared imaging is obtained. The Otsu threshold method is applied from the histogram to obtain a parameter of optimal threshold (U_{opt}), which determines a relationship between the hot area region of infrared imaging and the remaining parts of the image through statistical methods that identify the ROI within the infrared image using automatic segmentation.

D. EXTRACTION

Temperature estimation in thermography is of vital importance to obtain accurate results. In this regard, different methodologies to correctly calculate temperature values are proposed in the literature; the method most widely used by different camera manufacturers is based on radiation received by the camera that originates from three information sources: the objective, the environment, and the atmospheric and object-reflected emissions [39]. In the same way, infrared imaging can be used to calculate temperature values by means of the gray-scale pixel intensity values [40].

Unlike methodologies that use color images, this paper uses gray-scale infrared imaging. The gray-scale infrared images are 8-bit digital images, which means that the image is represented by gray level intensities ranging from 0 to 255. Working with this type of image facilitates data processing, allowing low computational complexity as well as reduced processing times, because the information in this type of image is reduced yet valuable compared with image color analysis. With the gray-scale infrared imaging intensity values and knowing both the maximum temperature Tc_{max} and the minimum temperature Tc_{min} obtained directly from the thermographic camera measurement and calculating the actual temperature values using (7), this equation is applied to gray-scale intensity matrices, since a digital gray-scale thermographic image can be represented by a matrix with intensity values ranging from 0 to 255 [40]. Through this process, for each pixel of infrared imaging in gray-scale, the true temperature (thermogram) is reached.

$$T_{true}(x, y) = Tc_{min} + \frac{T_{gray}(x, y)}{T_{mgv}} * (Tc_{max} - Tc_{min}) \quad (7)$$

where $T_{true}(x, y)$ is the value of the true temperature derived from the pixel intensity, Tc_{max} and Tc_{min} are the maximum and minimum temperature of the infrared imaging, respectively, $T_{gray}\ (x, y)$ is the value of the pixel intensity in the gray-scale image and T_{mgv} is the peak intensity value in the infrared imaging.

From the calculated thermogram, feature extraction is possible; this comes from the ROI detection determined by automatic image segmentation. For example, it is possible to extract T_{max}, T_{min} and the average temperature T_{avg}. Additionally, it is possible to apply a qualitative method to obtain the relative temperature ΔT (8) and the difference in temperature ΔTr (9) of the ROI of IM with faults and those of motors in healthy-condition subject to the same conditions.

TABLE 1. Parameters of interest.

N	Parameter	Symbol
1	Maximum temperature	T_{max}
2	Minimum temperature	T_{min}
3	Average temperature	T_{avg}
4	Temperature difference between target and reference region	ΔT
5	Temperature relative between target and reference region	ΔTr
6	Area segmentation region	A

$$\Delta T = T_{hot} - T_{ref} \quad (8)$$

$$\Delta T_r = \frac{T_{hot} - T_{ref}}{T_{ref}} * 100\% \quad (9)$$

where ΔT is the difference in temperature, ΔTr is the relative temperature, T_{hot} is the temperature of the ROI of the IM with a fault and T_{ref} is the temperature of the ROI of a healthy system. Table 1 shows a summary of the parameters calculated for every ROI obtained from automatic image segmentation.

Additionally, parameters based on first order statistics are proposed since they are widely used in the study of infrared imaging [30], providing information for the detection and fault diagnosis present in IM. The asymmetry of infrared imaging is described through histogram based first order statistical features. A histogram is a graphical representation of pixel distribution of an image. Average gray intensity, (10), skewness, (11), kurtosis, (12), entropy, (13), standard deviation, (14), and variance, (15) are obtained by a feature extraction for a failure analysis of infrared imaging. fx and gy indicate the number of pixel columns and number of pixel rows respectively, p is the number of distinct gray-scale pixels in the quantized image, h(p) is the histogram of the pixel intensity and q is the number of possible intensity levels of the image [41]. The feature extraction is expressed as follows:

$$\mu = \frac{1}{f_x g_y} \sum_{p=0}^{q-1} ph(p) \quad (10)$$

$$\frac{1}{\sigma^3 f_x g_y} \sum_{p=0}^{q-1} (p - \mu)^3 h\,(p) \quad (11)$$

$$\frac{1}{\sigma^4 f_x g_y} \sum_{p=0}^{q-1} (p - \mu)^4 h(p) \quad (12)$$

$$-\frac{1}{f_x g_y} \sum_{p=0}^{q-1} nlog(p) \quad (13)$$

$$\sigma = \left(\frac{1}{f_x g_y} \sum_{p=0}^{q-1} (p - \mu)^2 h\,(p)\right)^{\frac{1}{2}} \quad (14)$$

$$\sigma^2 = \frac{1}{f_x g_y} \sum_{p=0}^{q-1} (p - \mu)^2 h\,(p) \quad (15)$$

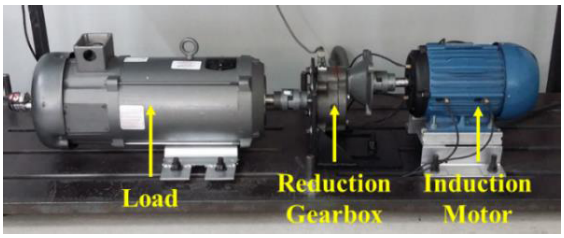

FIGURE 3. Testing bench with electromechanical system for the monitoring, detection and fault analysis of an induction motor using infrared imaging.

E. SEVERITY

A qualitative method is applied, in which IM with faults are compared to healthy IM operating under similar conditions to determine the temperature difference and to analyze the anomalies produced by high temperatures in the IM. The severity of the fault in the IM is estimated by obtaining the difference in temperature ΔT, and using the American Society for Testing & Materials Standard (ASTM E1934-99a) [42] we can estimate the severity of the fault that the IM may have.

IV. EXPERIMENTAL SETUP

The infrared imaging is conducted with an infrared camera (model FLIR A310, from FLIR Systems Incorporated) [43]. The thermographic camera was adjusted to obtain accurate results based on different environmental factors such as emissivity, atmospheric temperature, relative humidity, reflected temperature and the distance between the IM and the camera. The value of the emissivity is calculated by means of empirical tests through a supervised adjustment as explained in the methodology of this work, the emissivity value is adjusted to 0.93, which is used for all the tests carried out in this work. This value is in the proposed ranges suggested for painted surfaces and recommended in previous works related to electrical systems [44], [45] and was adjusted by tests. Furthermore, the Fluke 975 AIMETER and the Fluke 61 were employed to measure the environmental parameters for each test. The algorithms for automatic image segmentation, the calculation of the thermogram, the features extraction, and the qualitative method are programing in C++. An electromechanical system consisting of an AC machine, a 1.5 kW induction motor, WEG three-phase electric power, connected to 220 V_{AC} at 60 Hz is used for the conducted tests. The IM is mechanically coupled to a gearbox by a rigid coupling, a reduction gearbox and an electric generator representing the mechanical load of the system. Fig. 3 shows the configuration of the system under test.

The purpose of this methodology is monitoring the thermal behavior in the IM for a HLT condition and under different fault conditions such as a BRB, BD and MAL, to obtain suitable patterns to differentiate among motor conditions. The BRB condition is simulated by drilling the rotor to an 8 mm depth to break one rotor bar as shown in Fig. 4a. A 2 mm hole is drilled on the outer race of the bearing for the BD condition,

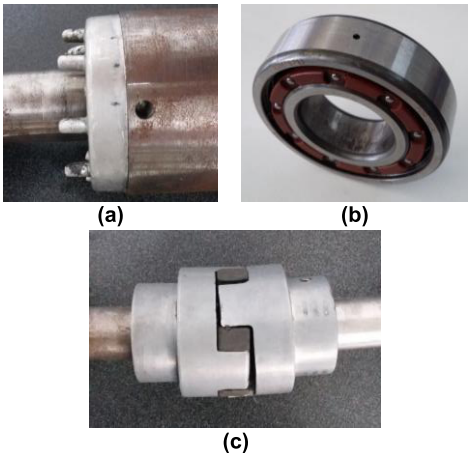

FIGURE 4. Proposed study cases for infrared imaging-based fault analysis: a) Broken rotor bar (BRB), produced by drilling the rotor 8 mm, b) Ball bearing defect (BD), produced by drilling a 2 mm hole, and c) Misalignment (MAL), producing by moving the free end of the induction motor.

as shown in Fig. 4b. The MAL condition is produced by moving the free end of the IM so that a misalignment of 5 mm in the horizontal plane is produced only from the free end; Fig. 4c shows the misalignment on the shaft coupling.

Four experimental conditions are studied on the IM: HLT, BRB, BD and MAL. Each test lasted 80 minutes; since in this time the healthy motor reached thermal stability. The image capture period for infrared imaging was one each minute, so at the end of every test 80 infrared images were obtained. For each case study proposed in this work, five different tests were carried out. The proposed methodology uses two infrared imaging captures from each test for its thermal analysis, the first obtained at the start of the test and the second obtained 80 minutes after starting the test.

V. RESULTS AND DISCUSSION

Fig. 5 shows the infrared images that are obtained as a final result of the monitoring the IM for the proposed study cases. Although the infrared imaging is shown in pseudocolor for better visualization, the proposed methodology employs gray-scale infrared imaging, which is also provided by the thermographic camera. Fig. 5a shows an infrared imaging of the healthy condition obtained when the IM reached thermal stability. Fig. 5b depicts the BRB condition in the electric machine; Fig. 5c shows the infrared imaging for the BD; and Fig. 5d depicts the MAL condition. These results from the infrared imaging show a remarkable difference between the study cases.

Once the thermal behavior of the rotating machine is obtained from the infrared imaging, the Otsu threshold method is applied for image segmentation since it provides good results for ROI detection, which is one of the contributions of this work. The threshold reference is established by the HLT condition as shown in Fig. 6a. Afterwards, the Otsu threshold method is applied, and for this case, the optimal

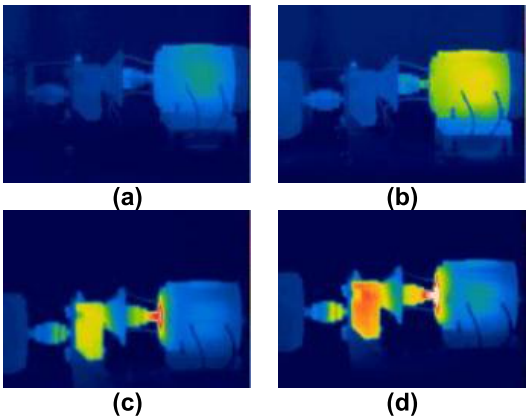

FIGURE 5. Infrared imaging of the electromechanical system for fault analysis in the induction motor: a) Healthy motor (HLT), b) Broken rotor bar (BRB), motor induction fault condition, c) Ball bearing defect (BD), motor induction fault condition, and d) Misalignment (MAL), motor induction fault condition.

threshold parameter is $U_{opt} = 76$. Fig. 6b shows the thresholding of the gray-scale healthy system. Then, the different cases of study are analyzed using the proposed methodology. The BRB condition is analyzed with Otsu threshold method, obtaining an optimal threshold of $U_{opt} = 103$. Fig. 6c shows the gray-scale infrared imaging and Fig. 6d depicts the thresholding. In the same way, the BD failure is processed with the Otsu threshold method, obtaining an optimal threshold of $U_{opt} = 141$. The gray-scale image is shown in Fig. 6e and the thresholding is obtained as depicted in Fig. 6f. Finally, the MAL condition is also processed, obtaining an optimal threshold of $U_{opt} = 82$. The gray-scale image for the misalignment condition is shown in Fig. 6g and Fig. 6h depicts the thresholding.

From (4) and with the values of the maximum and minimum temperature of each infrared imaging, the temperature matrix (thermogram) is calculated. Fig. 7 shows the results obtained from the automatic image segmentation applied to the infrared imaging for each study case proposed in this work. With the thermogram and the segmented infrared imaging, the thermal behavior of the induction motor is obtained for each test carried out, applying feature extraction to the ROI (Table 1).

By applying the proposed methodology, the parameters of interest are obtained to estimate the thermal behavior produced by the IM under different conditions. First, the healthy condition is compared to the other conditions with faulty states. Next, a qualitative method is applied, which consists of comparing the IM in a healthy state to the system when it is faulty; using the ASTM E1934-99a standard, the operating condition of the IM is estimated. Table 2 shows the results of the parameters of interest for all study cases. The system with a BRB has a temperature difference of 7.86 °C while the HLT condition results in an increase in temperature of 26.78%.

The image segmentation shown in Fig. 7a and Fig. 7b demonstrates how the heat is distributed throughout the electric machine and may affect other elements of the motor

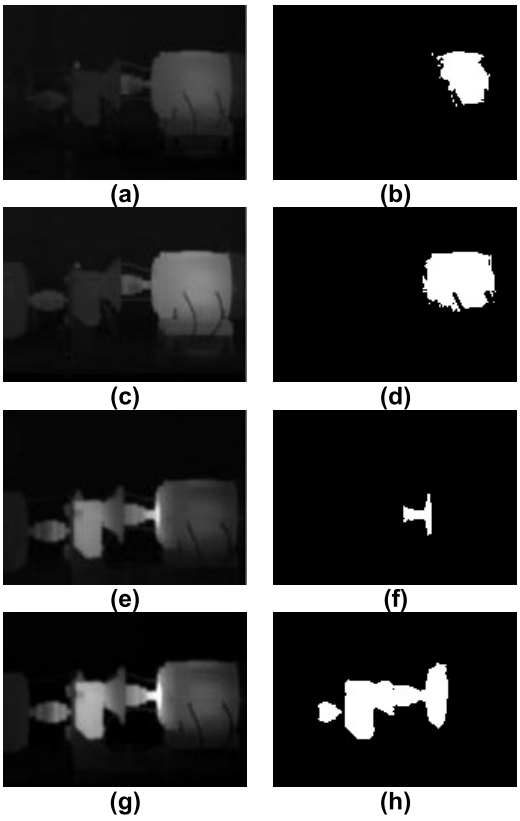

FIGURE 6. a) Gray-scale infrared imaging of a healthy system (HLT), b) Applying automatic thresholding to a healthy system (HTL), c) Gray-scale infrared imaging of a broken rotor bar system (BRB), d) Applying automatic thresholding to broken rotor bar system (BRB), e) Gray-scale infrared imaging of ball bearing defect system (BD), f) Applying automatic thresholding to ball bearing defect system (BD), g) Gray-scale infrared imaging of a misaligned system (MAL) and h) Applying automatic thresholding to a misaligned system (MAL).

TABLE 2. Features of Interest for fault diagnostic.

Type of System	Features				
	T_{max} (°C)	T_{min} (°C)	T_{avg} (°C)	ΔT (°C)	ΔT_r (%)
Healthy (HTL)	29.35	20.87	24.20	-	-
Broken Rotor Bar (BRB)	37.21	21.67	30.44	7.86	26.78
Bearing Defect (BD)	46.54	26.92	34.73	17.19	58.57
Misalignment (MAL)	40.24	24.18	32.23	10.89	37.10

such as the windings. The BD condition reaches a maximum temperature of 46.54 °C with a temperature difference of 17.19 °C compared to the HLT system, an increase of 58.57%. The image segmentation from Fig. 7c clearly shows that the area where the heating occurs is where the damaged ball bearing is located. In this case, the heating is concentrated at a specific area near the bearing. Finally, the MAL condition reaches a maximum temperature of 40.24 °C, a temperature difference of 10.89 °C compared to the HLT system, which represents a 37.10% increase. The image segmentation from Fig. 7d clearly shows that the area where the heating occurs is where the misalignment is present, in this case in the coupling of the induction motor

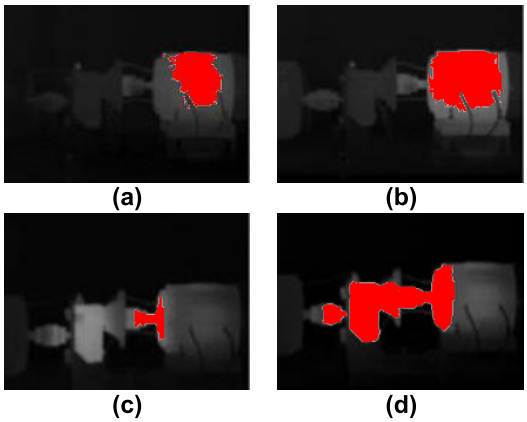

FIGURE 7. Automatic segmentation of infrared imaging. The red-colored areas represent the location of the heating produced by each failure case studied in this paper: a) Healthy (HLT), b) Broken Rotor Bar (BRB), c) Ball Bearing Defect (BD), and d) Misalignment (MAL).

TABLE 3. First order statistical features.

Parameter	HTL	BRB	BD	MAL
Average	24.200	30.440	34.730	32.230
Standard deviation	2.760	2.3800	4.800	6.770
Variance	7.610	5.660	23.040	45.830
Skewness	0.522	0.004	0.065	0.080
Kurtosis	1.850	0.460	0.390	1.040

shaft with the gearbox. The thermal pattern is clearly differentiated from the healthy condition pattern. Also, the thermal patterns are different for each study case, which helps identify the fault.

A thermal analysis was performed on the information provided by the gray-scale infrared imaging, obtaining the first order statistical parameters as shown in Table 3. The results show an increase in the average temperature which varied with failure analysis. For example, when the IM has a BRB failure, the temperature increase is 25.78%; with the BD failure, it increases 43.51%; and with a MAL fault, it increases 33.18%, all compared with the HLT condition. While kurtosis and skewness decrease in the study of the faults, when the IM has a BRB failure, there is a decrease of 75.13%; with a BD failure, it decreases 78.91%; and with a MAL fault, it reduces by 43.78%. With these results, it is possible to consider the average temperature increase, the kurtosis and the skewness as parameters for fault location and fault diagnosis in IMs.

With the obtained results, the reached heating temperatures can be analyzed through the international standard for manual classification of conditions in electrical equipment, ASTM E1934-99a, in which an action is recommended to be undertaken depending on the temperature difference (ΔT) obtained by a quantitative analysis between a healthy system and a system with faults under the same operating conditions. Table 4 summarizes the standard for classifying conditions in electrical equipment.

TABLE 4. Conditions of qualitative measurement.

Priority	ΔT (°C)	Recommended action
I	$\Delta T \geq 15$	Major discrepancy, Repair immediately
II	$5 < \Delta T < 15$	Indicate probable deficiency, Repair as time permits
III	$\Delta T \leq 5$	Possible deficiency, Warrants investigation

TABLE 5. Comparative analysis.

Type of System	A (Pixel)	ΔT_r (%)	Comparative
Healthy (HTL)	1451	-	HTL has a temperature maximum of 29.35 °C and a heating area of 1451 pixel, which is distributed in a part of the motor body.
Broken Rotor Bar (BRB)	1917	26.78	BRB has a temperature increase of 26.78% and the heating area increment to 32.1%, which is distributed by all the motor body.
Bearing Defect (BD)	614	58.57	BD has a temperature increase of 58.57% and the heating area is 57.6% smaller, but it is concentrated at a specific area near the bearing.
Misalignment (MAL)	1587	37.10	MAL has a temperature increase of 37.10% and the heating area increment to 9.3%, however, it is present in the coupling of the motor shaft with the gearbox.

Following the methodology proposed in this work, the fault severity is estimated at the induction motor. According to the standard, the BD fault has a large discrepancy with respect to the healthy condition and it should be repaired immediately. The BRB fault is classified as priority II and is recommended for repair when time permits. Finally, the MAL condition is classified the same as the BRB fault, indicating a probable deficiency which is recommended for repair when time permits.

Table 5 shows a comparison of the heat distribution and the temperature from a qualitative analysis. The electric machine in a healthy state is compared with each fault case studied in this paper. The increase in temperature of the IM, due to different faults has consequences that affect the IM, such as considerable wear on its elements and the kinematic chain which eventually reduces the rotating machine's life. Additionally, depending on where the failure occurs, it can damage other elements; for example, when the IM has a BRB fault, the heat generated by the fault is dispersed throughout the induction motor, and it may damage the windings. When the fault is a BD, as observed in the results, it affects the area where the bearing is installed and may affect the motor shaft since the ball bearing is mounted on the shaft.

When there is a MAL fault, the heat distribution goes from the induction motor to the gearbox, which can cause wear on the elements of the kinematic chain or on the motor itself. These are some of the problems that directly affect the

TABLE 6. Features for fault diagnostic with commercial software.

Type of System	Features	$Bx1$ (ºC)	$Bx2$ (ºC)	$Bx3$ (ºC)
Healthy (HTL)	T_{max}	28.1	21.4	21.1
	T_{min}	19.2	18.7	18.6
	T_{avgs}	25.3	20.3	20.1
Broken Rotor Bar (BRB)	T_{max}	36.5	34.6	30.1
	T_{min}	20.8	20.3	19.8
	T_{avgs}	29.4	27.8	20.1
Bearing Defect (BD)	T_{max}	25.6	44.8	30.2
	T_{min}	21.8	20.2	18.9
	T_{avgs}	23.1	32.8	25.3
Misalignment (MAL)	T_{max}	27.3	39.2	36.8
	T_{min}	20.8	23.2	20.1
	T_{avgs}	22.4	29.5	28.8

system. However, it has been shown that an increase in temperature represents energy losses caused by faults, which can have major consequences such as an increase in the motor's energy consumption, decreased operational efficiency of the equipment, and higher operation expenses of the induction motor [3]. With the proposed methodology it is possible to conduct a thermal analysis based on temperature increase to identify the faults.

Finally, a comparison is made between the methodology proposed in this work and thermal analysis of infrared imaging using commercial software, to determine the advantages of the methodology proposed in this work. The infrared imaging of Fig. 5 were processed with the FLIR Tools software, and manually segmented as shown in Fig. 8, obtaining the maximum temperature (T_{maxs}), minimum temperature (T_{mins}) and temperature average (T_{avgs}) as parameters of interest in each segmented region. The results are obtained with the commercial software are shown in Table 6.

The methodology proposed in this work can be considered an attractive and alternative tool for classical infrared imaging inspection procedures and for techniques of IM monitoring and failure analysis, due to the advantages it offers compared to the use of commercial software. One advantage is that the proposed methodology monitors, detects, extracts, analyzes and performs fault diagnosis in an IM automatically, without the need of operator interpretation, reducing data processing times. This contrasts with using commercial software, which requires qualified personnel for interpretation and analysis of the infrared image. Another advantage of the proposed methodology is the feature extraction of features of interest such as T_{max}, T_{min}, T_{avg}, ΔT, ΔTr, and first-order statistics (Table 2 and 3) of the ROI, with which a more complete failure analysis and diagnosis can be conducted. Conversely,

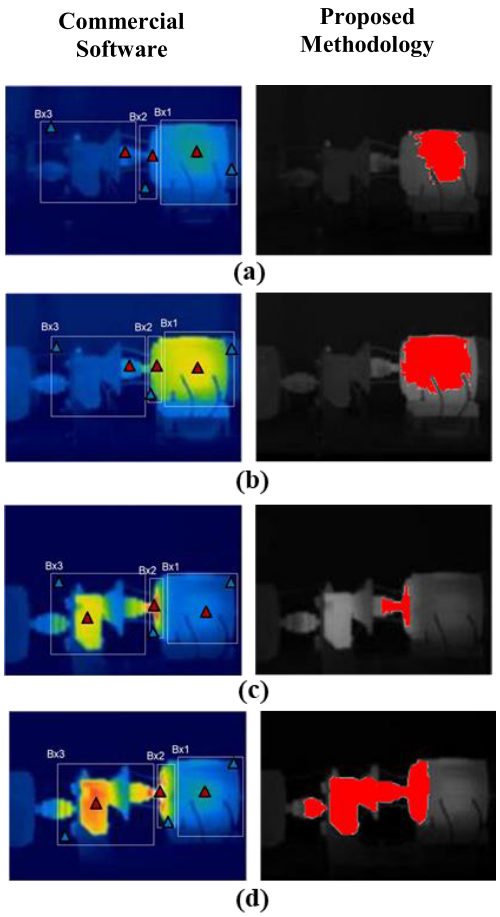

FIGURE 8. The images in the left column represent the infrared imaging segmented with commercial software, while the infrared imaging in the right column shows the results of the automatic segmentation proposed in this paper, a) Healthy (HLT), b) Broken Rotor Bar (BRB), c) Ball Bearing Defect (BD), and d) Misalignment (MAL).

the majority of commercial software only obtains T_{max}, T_{min}, and T_{avg} of the ROI (Table 4) for thermal analysis.

The values obtained in Table 4 are acceptable for IM failure analysis, but are subject to errors because T_{max} and T_{min} are parameters that represent a single image pixel. Sometimes these values can be image noise and not the exact actual temperature. In addition, the image segmentation zone is larger, involving regions that are not of interest for the thermal analysis, having a different T_{avg}. To reduce these problems that often arise when analyzing infrared imaging with commercial software, this methodology proposes a statistical analysis with the parameters obtained directly from the ROI, which allows a greater veracity in the failure analysis and fault diagnosis. Another advantage is that based on the automatic image segmentation of the ROI, the type of IM fault condition (HTL, BRB, BD, and MAL) is determined, since they are represented by the hot spots generated by the faults. Studies in the literature have reported that the area where there is considerable warming in the IM or the kinematic chain can be related to failure type [25], [37], [38]. Conversely, with commercial software, image segmentation is

done manually and empirically, basing the fault classification on the operator's experience. Another advantage is that the methodology has the capacity to determine the severity of the failure and make a recommendation for the maintenance action to be followed, using the ASTM E1934-99a standard, a methodology based on a standard that is widely approved for the detection of anomalies in rotating machines from infrared imaging. Finally, the proposed methodology is an open architecture allowing the improvement and development of new algorithms that make this method more robust, in contrast with most commercial software, which cannot be developed because they have a closed software architecture.

Despite its advantages, the methodology proposed in this paper has some limitations in industrial application. First, it is dependent on the prior knowledge of the IM thermal conditions; second, it does not allow analysis of all the different points of the infrared imaging because it focuses on the ROI, which contains the hottest areas of the infrared imaging. Nevertheless, these limitations can be compensated for by using other approved techniques for IM failure analysis, such as analysis by MCSA or vibration. Finally, another limitation is to consider the minimum set of criteria necessary to capture infrared imaging (focusing, reflection, light, emissivity, reflected object and atmospheric temperatures, and relative humidity), but it is possible to include sensors that help measure these parameters.

VI. CONCLUSIONS

This article presents an automatic methodology for the monitoring, detection, extraction, and failure analysis in an IM using thermographic images. This method can be considered an attractive and alternative tool due to its faster data processing compared to manual methods that use infrared imaging. In addition, it is a standard-based methodology (based on the ASTM E1934-99a standard) approved for failure analysis in rotating machines using infrared imaging.

This methodology has been tested to detect abnormal thermal conditions in three defective conditions present in an induction motor; a broken rotor bar, ball bearing defects and misalignment. From the results, it can be concluded that the proposed methodology is adequate for fault diagnosis for the faults considered, as well as to effective in determining the severity of the failure and a recommendation on the immediacy of the corrective actions required.

Based on the results of the proposed methodology and the literary review, it can be concluded that this work can greatly help or complement the techniques used most frequently in fault analysis, and as a result a more complete analysis for the detection of faults in an IM and the kinematic chain can be obtained.

The results obtained in this work suggest that this methodology is well adapted for fault location in IM and it can be extended for monitoring the operating conditions of the associated kinematic chain. Future works will implement an automatic faults classifier based on pattern recognition methods applied to the image segmentation.

REFERENCES

[1] C. N. Jibhakate, M. A. Chaudhari, and M. M. Renge, "Reactive power compensation using induction motor driven by nine switch AC-DC-AC converter," *IEEE Access*, vol. 6, pp. 1312–1320, 2018.
[2] M. A. Hannan *et al.*, "A quantum lightning search algorithm-based fuzzy speed controller for induction motor drive," *IEEE Access*, vol. 6, pp. 1214–1223, 2018.
[3] F. Giri, *AC Electric Motors Control: Advanced Design Techniques and Applications*. Hoboken, NJ, USA: Wiley, 2013.
[4] V. Leemans, M.-F. Destain, B. Kilundu, and P. Dehombreux, "Evaluation of the performance of infrared thermography for on-line condition monitoring of rotating machines," *Engineering*, vol. 3, pp. 1030–1039, Oct. 2011.
[5] D. A. Tobon-Mejia, K. Medjaher, and N. Zerhouni, "CNC machine tool's wear diagnostic and prognostic by using dynamic Bayesian networks," *Mech. Syst. Signal Process.*, vol. 28, pp. 167–182, Apr. 2012.
[6] M. Valtierra-Rodriguez, R. de Jesus Romero-Troncoso, R. A. Osornio-Rios, and A. Garcia-Perez, "Detection and classification of single and combined power quality disturbances using neural networks," *IEEE Trans. Ind. Electron.*, vol. 61, no. 5, pp. 2473–2482, May 2014.
[7] Y. Shatnawi and M. Al-Khassaweneh, "Fault diagnosis in internal combustion engines using extension neural network," *IEEE Trans. Ind. Electron.*, vol. 61, no. 3, pp. 1434–1443, Mar. 2014.
[8] M. J. Picazo-Ródenas, R. Royo, J. Antonino-Daviu, and J. Roger-Folch, "Use of the infrared data for heating curve computation in induction motors: Application to fault diagnosis," *Eng. Failure Anal.*, vol. 35, pp. 178–192, Dec. 2013.
[9] Z. Xu, C. Hu, F. Yang, S.-H. Kuo, C.-K. Goh, and S. Nadarajan, "Data-driven inter-turn short circuit fault detection in induction machines," *IEEE Access*, vol. 5, pp. 25055–25068, 2017.
[10] S. Ul Haq and T. Bashir, "Evaluation of induction motor groundwall insulation using infrared thermography," presented at the 2nd Int. Conf. Emerg. Technol. (IEEE-ICET), Peshawar, Pakistan, Nov. 2006.
[11] C. Bougriou, R. Bessaïh, R. Le Gall, and J. C. Solecki, "Measurement of the temperature distribution on a circular plane fin by infrared thermography technique," *Appl. Thermal Eng.*, vol. 24, nos. 5–6, pp. 813–825, 2004.
[12] S. Bagavathiappan, B. B. Lahiri, J. Philip, T. Saravanan, and T. Jayakumar, "Infrared thermography for condition monitoring—A review," *Infr. Phys. Technol.*, vol. 60, pp. 35–55, Sep. 2013.
[13] C. A. Balaras and A. A. Argiriou, "Infrared thermography for building diagnostics," *Energy Buildings*, vol. 34, no. 2, pp. 171–183, 2002.
[14] Z. Ge, X. Du, L. Yang, Y. Yang, Y. Li, and Y. Jin, "Performance monitoring of direct air-cooled power generating unit with infrared thermography," *Appl. Thermal Eng.*, vol. 31, no. 4, pp. 418–424, 2011.
[15] D. J. Titman, "Applications of thermography in non-destructive testing of structures," *NDT E Int.*, vol. 34, no. 2, pp. 149–154, 2001.
[16] M. J. Picazo-Ródenas, R. Royo, J. Antonino-Daviu, and J. Roger-Folch, "Energy balance and heating curves of electric motors based on infrared thermography," presented at the Int. Symp. Ind. Electron. (IEEE-ISIE), Jun. 2011.
[17] M. J. Picazo-Ródenas, R. Royo, J. Antonino-Daviu, and J. Roger-Folch, "Use of infrared thermography for computation of heating curves and preliminary failure detection in induction motors," presented at the 20th Int. Conf. Elect. Mach. (IEEE-ICEM), Peshawar, Pakistan, Sep. 2012.
[18] A. G. Garcia-Ramirez, L. A. Morales-Hernandez, R. A. Osornio-Rios, J. P. Benitez-Rangel, A. Garcia-Perez, and R. de Jesus Romero-Troncoso, "Fault detection in induction motors and the impact on the kinematic chain through thermographic analysis," *Electr. Power Syst. Res.*, vol. 114, pp. 1–9, Sep. 2014.
[19] D. Lopez-Perez and J. Antonino-Daviu, "Application of infrared thermography to fault detection in industrial induction motors: Case stories," presented at the Int. Conf. Elect. Machines (IEEE-ICEM), Sep. 2016.
[20] A. Siddique, G. S. Yadava, and B. Singh, "A review of stator fault monitoring techniques of induction motors," *IEEE Trans. Energy Convers.*, vol. 20, no. 1, pp. 106–114, Mar. 2005.
[21] G. Singh and V. N. A. Naikan, "Infrared thermography based diagnosis of inter-turn fault and cooling system failure in three phase induction motor," *Infr. Phys. Technol.*, vol. 87, pp. 134–138, Dec. 2017.
[22] A. G. Garcia-Ramirez, L. A. Morales-Hernandez, R. A. Osornio-Rios, A. Garcia-Perez, and R. J. Romero-Troncoso, "Thermographic technique as a complement for MCSA in induction motor fault detection," presented at the IEEE Int. Conf. Elect. Mach. (IEEE-ICEM), Sep. 2014.
[23] P. Karvelis *et al.*, "An automated thermographic image segmentation method for induction motor fault diagnosis," presented at the 40th Annu. Conf. IEEE Ind. Electron. Soc. (IEEE-IECON), Oct./Nov. 2014.

[24] M. Eftekhari, M. Moallem, S. Sadri, and M.-F. Hsieh, "A novel indicator of stator winding inter-turn fault in induction motor using infrared thermal imaging," *Infr. Phys. Technol.*, vol. 61, pp. 330–336, Nov. 2013.
[25] E. Resendiz-Ochoa, J. P. Benitez-Rangel, R. A. Osornio-Rios, and R. J. Romero-Troncoso, "Segmentation in thermography images for bearing defect analysis in induction motor," presented at the Int. Symp. Diagnostics Electr. Mach., Power Electron. Drives (IEEE-SDEMPED), Aug./Sep. 2017.
[26] A. Glowacz and Z. Glowacz, "Diagnosis of the three-phase induction motor using thermal imaging," *Infr. Phys. Technol.*, vol. 81, pp. 7–16, Mar. 2017.
[27] S. Pramanik, D. Bhattacharjee, and M. Nasipuri, "Wavelet based thermogram analysis for breast cancer detection," in *Proc. Int. Symp. Adv. Comput. Commun. (ISACC)*, 2015, pp. 205–212.
[28] M. Win, A. R. Bushroa, M. A. Hassan, N. M. Hilman, and A. Ide-Ektessabi, "A contrast adjustment thresholding method for surface defect detection based on mesoscopy," *IEEE Trans. Ind. Informat.*, vol. 11, no. 3, pp. 642–649, Jun. 2015.
[29] T. Dutta, J. Sil, and P. Chottopadhyay, "Condition monitoring of electrical equipment using thermal image processing," in *Proc. IEEE 1st Int. Conf. Control, Meas. Instrum. (CMI)*, Jan. 2016, pp. 311–315.
[30] A. S. N. Huda and S. Taib, "Suitable features selection for monitoring thermal condition of electrical equipment using infrared thermography," *Infr. Phys. Technol.*, vol. 61, pp. 184–191, Nov. 2013.
[31] M. Vollmer and K. P. Möllman, "*Infrared Thermal Imaging: Fundamentals, Research and Applications*. Hoboken, NJ, USA: Wiley, 2010.
[32] M. Barański and A. Polak, "Thermographic diagnostic of electrical machines," *Przegląd Elektrotechn. (Elect. Rev.)*, vol. 33, p. 2097, Oct. 2011.
[33] P. Soille, *Morphological Image Analysis: Principles and Applications*, 2nd ed. Springer, 2002.
[34] R. M. Haralick and L. G. Shapiro, "Image segmentation techniques," *Comput. Vis., Graph., Image Process.*, vol. 29, no. 1, pp. 100–132, 1985.
[35] N. R. Pal and S. K. Pal, "A review on image segmentation techniques," *Pattern Recognit.*, vol. 26, no. 9, pp. 1277–1294, 1993.
[36] N. Otsu, "A threshold selection method from gray-level histograms," *IEEE Trans. Syst., Man, Cybern.*, vol. SMC-9, no. 1, pp. 62–66, Jan. 1979.
[37] P. Zhang, Y. Du, T. G. Habetler, and B. Lu, "A survey of condition monitoring and protection methods for medium-voltage induction motors," *IEEE Trans. Ind. Appl.*, vol. 47, no. 1, pp. 34–46, Jan./Feb. 2011.
[38] J. Faiz and M. Ojaghi, "Different indexes for eccentricity faults diagnosis in three-phase squirrel-cage induction motors: A review," *Mechatronics*, vol. 19, no. 1, pp. 2–13, 2009.
[39] R. Usamentiaga, P. Venegas, J. Guerediaga, L. Vega, J. Molleda, and F. G. Bulnes, "Infrared thermography for temperature measurement and non-destructive testing," *Sensors*, vol. 14, no. 7, pp. 12305–12348, 2014.
[40] Y.-C. Chou and L. Yao, "Automatic diagnostic system of electrical equipment using infrared thermography," presented at the Int. Conf. Soft Comput. Pattern Recognit., 2009.
[41] B. Wiecek, M. Strzelecki, T. Jakubowska, and C. Drews-Peszynski, *Advanced Thermal Image Processing*. Łódź, Poland: Tech. Univ. Lodz, Taylor and Francis Group, 2006.
[42] *Standard Guide for Examining Electrical and Mechanical Equipment With Infrared Thermography*, Standard ASTM E1934-99a, 2010.
[43] (May 20, 2018). *Infrared Thermography Camera FLIR 410a*. [Online]. Available: http://www.flir-webshop.com/en/electrical-mechanical/flir-i3-130.html
[44] G. J. Tattersall, "Infrared thermography: A non-invasive window into thermal physiology," *Comparative Biochem. Physiol. A, Mol. Integr. Physiol.*, vol. 202, pp. 78–98, Dec. 2016.
[45] A. S. N. Huda, S. Taib, M. Sha, and D. Ishak, "A semi-automatic approach for thermographic inspection of electrical installations within buildings," *Energy Buildings*, vol. 55, pp. 585–591, Dec. 2012.

EMMANUEL RESENDIZ-OCHOA received the B.E. degree in electromechanical engineering and the M.E. degree in mechatronics from the Autonomous University of Queretaro (UAQ), Queretaro, Mexico, in 2012 and 2015, respectively, where he is currently pursuing the Ph.D. degree with the Engineering Faculty. His research interests include image processing, computer vision, fault diagnosis in electromechanical systems, fault detection algorithms, and artificial intelligence.

ROQUE A. OSORNIO-RIOS (M'10) received the Ph.D. degree in mechatronics from the Autonomous University of Queretaro, Queretaro, Mexico, in 2007. He is a National Researcher level 2 with the Mexican Council of Science and Technology, CONACYT. He is currently a Head Professor with the Autonomous University of Queretaro. He has been an advisor for more than 80 theses, and a co-author of more than 90 technical papers published in international journals and conferences. His fields of interest include hardware signal processing and mechatronics. He is a fellow of the Mexican Academy of Engineering. He is a part of the Editorial Board of the *Journal of Scientific and Industrial Research*.

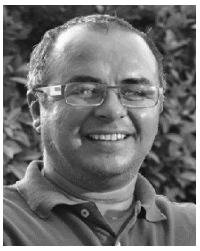

JUAN PRIMO BENITEZ-RANGEL received the degree in electromechanical engineering, the M.Sc. degree in instrumentation and automatic control, and the Ph.D. degree in engineering from the Faculty of Engineering, University Autonomous of Queretaro, Mexico, in 1999, 2006, and 2009, respectively. He is currently a Head Professor with the Faculty of Engineering, University Autonomous of Queretaro, where he holds the electromechanical engineering and mechatronics master's position. His research interests are in the fields of image processing and manufacture process. He has co-authored over15 technical papers published in international journals and conferences.

RENE DE J. ROMERO-TRONCOSO (M'07–SM'12) received the Ph.D. degree in mechatronics from the Autonomous University of Queretaro, Queretaro, Mexico, in 2004. He is a National Researcher level 3 with the Mexican Council of Science and Technology, CONACYT. He is currently a Head Professor with the University of Guanajuato and an Invited Researcher with the Autonomous University of Queretaro. He has been an advisor for more than 200 theses, an author of two books on digital systems (in Spanish), and a co-author of more than 130 technical papers published in international journals and conferences. His fields of interest include hardware signal processing and mechatronics. He was a recipient of the 2004 Asociación Mexicana de Directivos de la Investigación Aplicada y el Desarrollo Tecnológico, the National Award on Innovation for his work in applied mechatronics, and the 2005 IEEE ReConFig Award for his work in digital systems. He is a part of the Editorial Board of *International Journal of Manufacturing Engineering* (Hindawi).

LUIS ALBERTO MORALES-HERNANDEZ received the degree in electromechanical engineering, the M.Sc. degree instrumentation and automatic control, and the Ph.D. degree in engineering from the Faculty of Engineering, University Autonomous of Queretaro, Mexico, in 2004, 2005, and 2009, respectively. He is currently a Head Professor with the Faculty of Engineering, University Autonomous of Queretaro, where he holds electromechanical engineering and mechatronics master's and doctoral positions, respectively. He is involved in some governmental projects and technology transfer contracts to industry. His research interests are in the fields of image processing, pattern recognition, and computer vision. He received the Best Thesis Award in engineering for his Ph.D.